**Proceedings of the 2007 IEEE/RSJ International
Conference on Intelligent Robots and Systems
San Diego, CA, USA, Oct 29 - Nov 2, 2007**

WeC3.6

Moth Plume-Tracing Derived Algorithm for Identifying Chemical Source in Near-Shore Ocean Environments

Wei Li

Department of Computer Science, California State University, Bakersfield
Bakersfield, CA 93311 USA
(wli@cs.csubak.edu)

Abstract – **This paper derives a single chemical sensor based algorithm from the moth-inspired chemical plume strategies for identifying plume sources in fluid-advected environments. We evaluate the algorithm performance using a simulated plume with significant meander and filament intermittency. The in-water test runs demonstrated the algorithm effective and robust to the variation of near-shore ocean environments.**

*Index Term*s — **Biologically inspired robots, autonomous underwater vehicles, odor source identification, chemical plume tracing, behavior-based control.**

I. INTRODUCTION

A central problem of chemical plume tracing (CPT) is to identify the odor source of a chemical plume transported in a fluid-advected environment by navigation of an autonomous underwater vehicle (AUV). Factors that complicate source identification include the unknown chemical source concentrations, chemical filament intermittency due to turbulent flow, and significant plume meander due to the flow variation with respect to both location and time. In order to develop an AUV based chemical plume tracer for natural fluid environment application, several biologically inspired CPT strategies were proposed [1]-[7] under the CPT program sponsored by DARPA/ONR. Some groups also presented and tested CPT algorithms using laboratory robots, e.g., [8]-[10]. All the above studies mainly focused on the plume tracing issue (travel distance or time cost from the first chemical detection point to a position near the source location), but they lacked detail discussion of the source identification issue.

Different from plume tracing, there is no clear analog to the AUV Declare-Source behavior for animals. For biological entities (e.g. moths), the conclusion of identifying the pheromone source location may still be a mystery. Instead, while the moth plume-tracing relies primarily on sensed pheromone, the final determination of the location of the female moth could be based on data from multiple sensors, including vision, tactile, or even auditory cues. However, for CPT in near-shore ocean environments using AUVs, the current state of technology requires that we determine the plume source location based only on locations of the chemical detection events. A straightforward idea of the source identification is to estimate the odor source based inter-hit distances of chemical detection points (odor-hit points) during plume tracing activities. The vehicle has ceased up the plume due to the inter-hit distances. Nonetheless, whether the vehicle has reached the source is

not foolproof, because inter-hit distances might occur in any part of the plume [6]. The inter-hit distances are sensitive to the sampling of the vehicle control system and the predefined concentration threshold of plume-tracing algorithms. In addition, the fluid mechanics studies show that, at medium and high Reynolds numbers, the evolution of the chemical distribution in the flow is turbulence dominated [11]. As a result, the turbulent diffusion process leads to a highly discontinuous and intermittent distribution of the chemical plume, which makes the source identification from the odor-hit points more arduous.

In order to perform the in-water test runs via a REMUS vehicle [12], [13], we derived a source identification algorithm from the moth-inspired plume-tracing strategies [7], [14]. Fig. 1 shows a CPT test run conducted in June 2003 in Duck, North Carolina, including Maintain-Plume, Reacquire-Plume, and Declare-Source activities. This paper systemically presents the process of designing, evaluating, and testing the source identification algorithm. First, we introduce the concept of last chemical detection points (LCDPs) to construct source identification zones (SIZs) and to develop a SIZ algorithm for source identification based on chemical detection events by integrating measured vehicle locations and instantaneous fluid flow directions. Second, we evaluate the algorithm using Monte Carlo methods in a simulated fluid flow environment [15]. Finally, we report the in-water test and draw some conclusions.
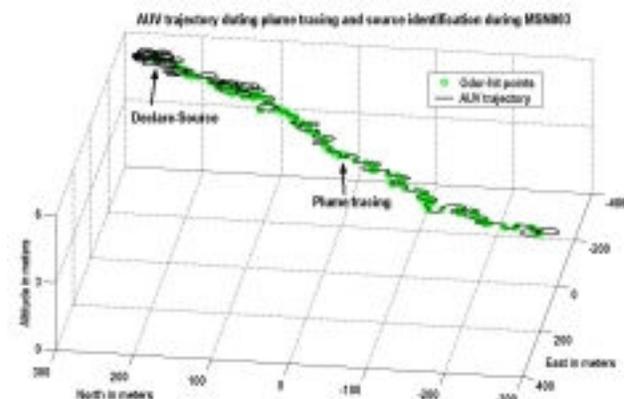

Fig. 1. An *active* moth-inspired plume tracing test conducted in near shore ocean conditions, in June 2003 in Duck, North Carolina. The Euclidian distance of plume tracing over 975 meters with source identification accuracy of approximately 13 meters
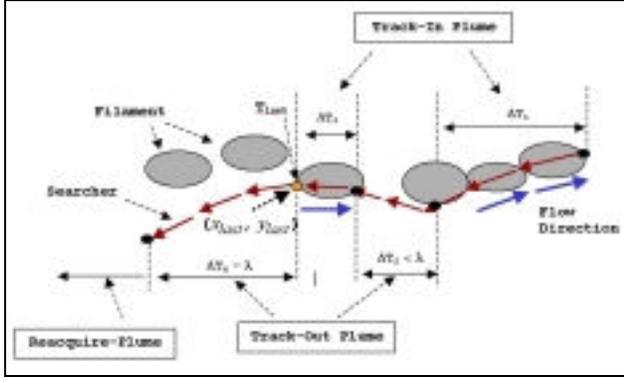
Fig. 2. Definition of a last chemical detection point

Fig. 3. Derivation of source identification algorithm from moth-inspired plume tracing strategies

II. DESIGN OF SOURCE IDENTIFICATION ALGORITHMS

A. Moth-inspired plume tracing strategies

We designed a subsumption architecture presented in [12] for CPT strategies and implemented it on the REMUS for the three sets of successful in-water tests. The architecture is composed of four primary behavior types: Find-Plume, Maintain-Plume, Reacquire-Plume, and Declare-Source. The source identification algorithm is derived from two moth-inspired behaviors: Maintain-Plume and Reacquire-Plume [16], [17]. Maintain-Plume is broken down into Track-In and Track-Out activities due to intermittency of a chemical plume transported in a fluid flow environment. Their commands (θ, ν) are defined

$$\theta = w_d(t, x_c, y_c) + 180° + \Delta\theta(t)_{\text{Track-In}}$$
$$\nu = \nu_c \tag{1}$$
$$t \in T_{above}$$

$$\theta = w_d(t, x_c, y_c) + 180° + \Delta\theta(t)_{\text{Track-Out}}$$
$$\nu = \nu_c \tag{2}$$
$$t \in T_{below}$$

where $\Delta\theta(t)_{\text{Track-In}}$ and $\Delta\theta(t)_{\text{Track-Out}}$ are the offset angles for Track-In and Track-Out, T_{above} and T_{below} are the durations for Track-In and Track-Out activities. The *passive* and *active* plume-tracing strategies were developed based on the definition of $\Delta\theta(t)_{\text{Track-In}}$ and $\Delta\theta(t)_{\text{Track-Out}}$ [7].

The commands (θ, ν) for Reacquire-Plume are defined

$$\theta = \text{actan}\, 2(y_i - y_c, x_i - x_c)$$
$$\nu = \nu_c \tag{3}$$

where (x_c, y_c) is the current vehicle location, and (x_i, y_i) is a subgoal located on **Cloverleaf** in [12]. The cloverleaf center is (x_{last}, y_{last}), where the plume is most recently detected, and the length of each leaf is defined by d_{leaf}. The detail discussions on Maintain-Plume and Reacquire-Plume can be found in [7], [11].

B. Last chemical detection point (LCDP)

The AUV alternatively utilizes Maintain-Plume and Reacquire-Plume in making progress towards the source location in the up-flow direction. In a typical scenario of plume tracing, the vehicle activates Track-In once it detects a chemical plume, e.g., the activities in ΔT_1 and ΔT_3 in Fig. 2. The vehicle continues Track-Out when it loses a contact with
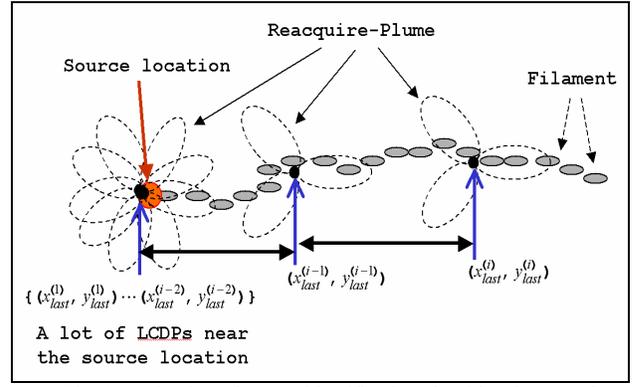
the chemical plume within λ seconds, e.g., the activity in ΔT_2 in Fig. 2. After λ seconds, it switches to Reacquire-Plume for casting the plume again on Cloverleaf trajectories, e.g., the activity in ΔT_4 in Fig. 2. A chemical detection point where the AUV loses the contact with the plume for λ seconds is defined as a last chemical detection point (LCDP), e.g., point (x_{last}, y_{last}) at T_{last} in Fig. 2. In order to develop the source identification algorithms, a LCDP node is defined by the structure

```
struct LCDP_Node
{
    double      Tlast, xlast, ylast;
    double      conc, fdir, fmag;
    double      xflow, yflow;
};
```

where T_{last} is the time when the LCDP is detected, (x_{last}, y_{last}) are the coordinates of the AUV at T_{last}, $conc$ is the chemical concentration at (x_{last}, y_{last}) and T_{last}, (f_{dir}, f_{mag}) are the flow direction and magnitude at (x_{last}, y_{last}) and T_{last}, and (x_{flow}, y_{flow}) are the coordinates of (x_{last}, y_{last}) in a new coordinate system, of which the x axis is aligned with the current flow direction. For convenience, we also use (x_{last}, y_{last}) to represent a LCDP in the following discussions. Note that $conc$ and f_{mag} in the node do not appear in the source identification algorithms, but they are reserved for possible further application. In our application, the chemical sensor works as a "binary detector". The Boolean value is "1" if the chemical concentration is above the threshold, while the Boolean value is "0" if the chemical concentration is below the threshold. The Monte Carlo study in [7] shows that decreasing the threshold increases the time the vehicle stays "in the plume", but accompanies an increase in noise. The threshold value was chosen as $conc > 4\%$ of the full scale (i.e., 0.2 V) based on an analysis of chemical sensor data in absence of the chemical. In this scenario, the sensor readings were pure noise, but never surpassed 0.2 V. The CPT strategies adopt this threshold for both the in-water tests and the simulation studies.

C. Patterns for source identification

LCDPs provide very important information about plume traversal distances among Reacquire-Plume activities. The LCDPs are separated along the plume axis when the AUV is far from the source location, while the LCDPs are clustered

in the vicinity of the source when the AUV is approaching the odor source, as shown in Fig. 3. The AUV usually exits the plume and moves up flow from the source when it traces the plume to the source location. After the AUV overshoots the odor source, it activates Reacquire-Plume to re-contact the plume on a Cloverleaf trajectory. As a result of frequently switching Maintain-Plume and Reacquire-Plume, the AUV generates a pattern with a number of Cloverleaf trajectories in the vicinity of the source location, as shown in figures 1 and 3. Such the distribution of LCDPs leads to development of a suitably close clustering of LCDPs for source identification.

The AUV detects a new LCDP and inserts its node into the list when the AUV switches its behaviors from Maintain-Plume to Reacquire-Plume. The list sorts the LCDP nodes in order of the current up-flow direction, $f_{dir}+180°$. In doing it, we define a new coordinate system. Its x axis is aligned with the f_{dir} direction and its origin is located at (x_{last}, y_{last}). The algorithm map each LCDP into the new coordinate system by

$$\begin{bmatrix} x_{flow} \\ y_{flow} \end{bmatrix} = \begin{bmatrix} \cos(f_{dir}+180°) & -\sin(f_{dir}+180°) \\ \sin(f_{dir}+180°) & \cos(f_{dir}+180°) \end{bmatrix} \begin{bmatrix} x_{last} \\ y_{last} \end{bmatrix}. \quad (4)$$

Their x_{flow} components determine the LCDP node priorities according to the current up-flow direction. The smallest x_{flow} has the highest priority. During CPT missions, the list accumulates LCDPs detected down-flow from the source location.

D. SIZ_M algorithm

The SIZ_M algorithm keeps updating the N_M most recent LCDPs, but sorts them in order of the current up-flow direction. SIZ_M is constructed by choosing a subset of the N_{dec} most up-flow LCDPs, where $N_{dec} \leq N_M$. This algorithm dynamically monitors the SIZ_M size. If the SIZ_M size is smaller than ε_M, the algorithm identifies the mean value of the LCDPs, $(x_{last}^{(m)}, y_{last}^{(m)})$, or the most up-flow LCDP, $(x_{last}^{f(1)}, y_{last}^{f(1)})$, as the source location. Table I lists the pseudo code of the SIZ_M algorithm. This algorithm has four parameters, the SIZ_M size criterion, ε_M, the integer, N_M, which indicates the constant number of LCDPs updated in the list, the integer, N_{dec}, the number of the most up-flow

Fig. 4. AUV identifies the source location in a fluid-advected environment

TABLE I
PSEUDO CODE FOR SIZ_M ALGORITHM

```
ALGORITHM SIZ_M( L[ 1,… N_M ] )
  //Identifying the source location by SIZ_M algorithm
  //Input: List L[ 1,…N_M ]
  //Output: Status of source identification
  if ( N_M ≥ N_ini )
      Sort L in order of the current up-flow direction
      Calculate SIZ_M box of N_dec LCDPs
      Calculate the diagonal R of SIZ_M
      if R ≤ ε_M

          return (x_last^(m), y_last^(m)) as the source location

      else
              return no source location identified
  else
          return no source location identified
```

LCDPs for source identification; and the initial value, N_{ini}. The SIZ_M version (ε_M =4 m, N_{dec}=3, $N_{ini}=N_M$=6) was implemented on the REMUS vehicle and successfully identified the plume sources during the three sets of in-water test runs.

III. SIMULATION EVALUATIONS

We evaluate the SIZ_M algorithm using the simulated plume [15], as shown in Fig. 4. The simulated plume model achieves significant computational simplification relative to turbulence models, but it was designed to maintain the plume characteristics that significantly complicate the plume tracing problems (intermittency, meander, and varying flow) caused by natural flow fluid. Instead of adjusting the Reynolds numbers, it controls a filament release rate (5–10 filaments/s) to simulate filament intermittency, addresses the meandering nature of the plume that is a key complicating factor to plume tracing, and manipulates flow varying that significantly challenges the CPT strategies. An operation area (OpArea) is specified by [0,100]×[-50,50] in meter. The simulation time step is 0.01 s. A source location is chosen at (20, 0) in meter, which allows us to check the accuracy of identified source location, but that location is unknown to the vehicle during CPT test runs. The dynamics model of the REMUS is implemented for simulation runs. The simulation environment is defined in the following way: first, the filament release rate is 5 filaments/s, because a low release rate may result in significant plume intermittency. This often causes the vehicle to lose contact with the plume and consequently to make spurious identifications. Second, the mean fluid velocity is 1 m/s. Fig. 5(a) illustrates flow velocity varying in [0.86, 1.17] m/s detected during a simulation run. The flow speed and flow variation, which are much larger than those detected during the in-water test runs, as plotted in Fig. 5(b), disperse the chemicals rapidly to challenge the efficacy and robustness of the plume-tracing strategies. Next, measured fluid direction is corrupted by additive noise from a white normal random process. For simulation runs, the vehicle velocity command is set at 1 m/s for Maintain-Plume. We use this speed, which is close to the mean fluid velocity, to evaluate if
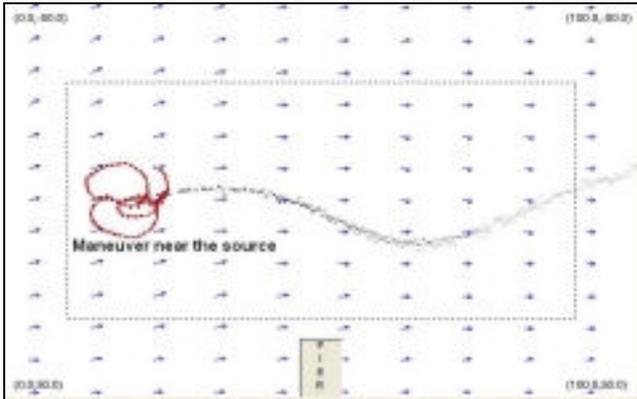
Track-Out activities turn the vehicle into the correct direction to encounter next chemical filament. The speed command for Reacquire-Plume is set at 1.4 m/s, which is slightly greater than the mean fluid velocity, to re-catch the lost plumes during Reacquire-Plume activities. The speed command of 2 m/s for Find-Plume allows the vehicle to explore the OpArea quickly.

An identified source location is valid, if its coordinates are situated within a given distance from a defined source location; otherwise it is invalid (spurious). For the evaluations, a valid source location is located within 10 meters from the defined source location. Accordingly, the identification time is the time spent maneuvering prior to identifying the source location after first approaching within the distance of the defined source location. We specify an initial location (80, -30) m for the evaluations. The Monte Carlo simulations continue 1000 CPT test runs, which is equivalent to keep consistently changing the plumes in the simulated fluid environments over 130 hours. This scale of days alters the relevant time scale for variations in the advected fluids and decay time for the vehicle, because there is no duplication of the trajectory, the odor-hit points, and the LCDPs from the 1000 test runs. We define a CPT test run as a complete cycle: the vehicle starts from and returns to its initial location. The test run fails if the vehicle cannot identify the source location within the time limit T_{max}=1000.0 s and records "over-time" for the test run; otherwise, the vehicle records the identification time, the total time for the test run, and the coordinates of the identified source location.

Table II list the source identification performance in three aspects: success rate, identification accuracy, and identification time. The SIZ_M algorithm achieves a high success rate of 96.8%. The result documents 31 spurious identifications and only one "over-time" run. The algorithm achieves the accuracy with the mean error of 2.92 m and the standard deviation of 1.53 m for the 1000 test runs. We summarize the distribution of the identified source locations in three groups: within 2 m, between 2 and 5 m, and between 5 and 10 m. 35.53% of the valid source locations fall within 2 m, 53.72% located between 2 and 5 m, and 10.95% between 5 m and 10 m. The algorithm averages the identification time of 104 s.

IV. IN-WATER TEST RESULTS

The SIZ_M algorithm was implemented on the REMUS AUV owned by SPAWAR in San Diego, CA, for the three sets of in-water test runs. The REMUS was modified to
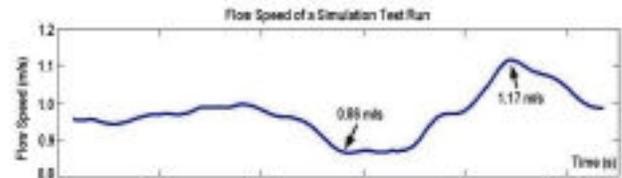
(a) Flow speed during a simulation run for t in [26.69, 234.30] s
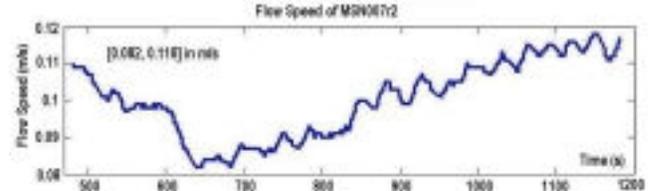
(b) Flow speed during the MSN007r2 mission for t in [480.3, 1190.6] s
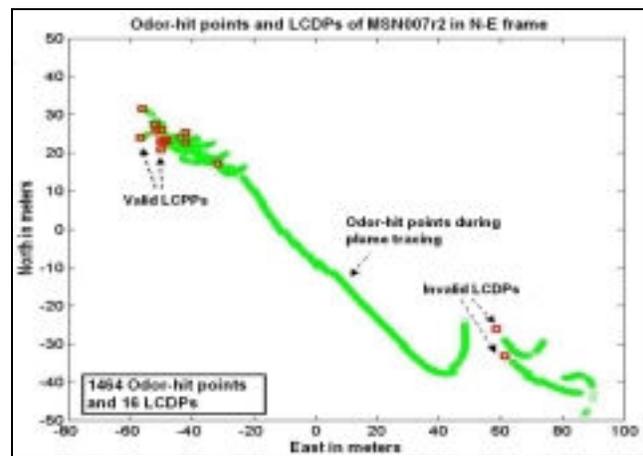Fig. 5. Comparison of flow speed and variation

contain a PC104 computer to run the CPT strategies. This computer received sensor data from the REMUS main computer via a serial connection, processed the sensor data, and supplied heading, speed, and depth/altitude commands to the main computer via the same serial connection. Up and down looking acoustic Doppler current profilers (ADCP) were onboard the REMUS. Finally, a fluorometer capable of detecting Rhodamine dye was mounted near the nose of the AUV. Rhodamine dye was used to create the plume for the experiments. The maximum speed of REMUS AUV is 2.6 m/s. The maximum turning rate of the vehicle is 15 degree/s. The guidance system limited the turning rate to 10 degree/s. The test director specified the OpAreas prior to the start of the mission and set the speed command for the vehicle at a constant value 1.5 m/s or 2.0 m/s prior to each run. The REMUS was launched from a boat on sea surface for the CPT missions, and traced the plume over 100 m toward the source below sea level from 5 m to 20 m. A video camera was in the water focusing on the chemical source to independently confirm source identification maneuvering. During the in-water runs, the Go-To module drove the AUV toward its identified source location at a lower altitude after having identified the plume source. The SIZ_M successfully completed the source identification for the last seven test runs labeled as MSN007r2 – MSN010r3 at SCI in 2002 [12]. This successful set of in-water test runs initiated two subsequent sets of the in-water tests at SCI in April and in Duck in June 2003. During these two in-water tests, the sidescan sonar imagery developed by the test team determined the true ground source location when the REMUS was maneuvering around the identified source location. During the field tests at SCI in April 2003, seven

TABLE II
SIMULATION EVALUATION OF SIZ_M ALGORITHM FOR THE TEST FIELDS

SIZ_M (1000 runs) (80, -30)	Success rate	Spurious identification / over-time	Mean and STD of identification error, meters	Error within 2 meters	Error within 2-5 meters	Error within 5-10 meters	Mean and STD of identification time, seconds
ε_M =4m N_{dec}= 3 N_M= 6 N_{ini} = 3	968 of 1000 (96.8 %)	31 of 1000 / 1 of 1000	$\Delta \overline{D}$ = 2.92m STD = 1.53m	342 of 968 (35.33%)	520 of 968 (53.72%)	106 of 968 (10.95%)	$\overline{T}_D$ = 104.0s STD = 40.6 s
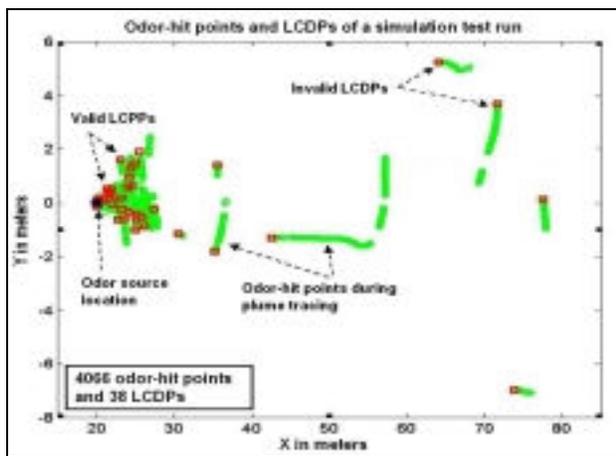
(a) 4066 Odor-hit points and 38 LCDPs detected during a simulation run   (b) 1464 Odor-hit points and 16 LCDPs detected during MSN007r2

Fig. 6. Distribution of odor-hit points and LCDPs

test runs successfully identified the source location with 8-17 m accuracy relative to the true ground. During the field tests in Duck in June 2003, the MSN003 mission identified the plume source with an error of approximately 13 m after tracing the plume over the Euclidian distance of 975 m in the specified OpArea by 367 x 1094 m (greater than 60 football fields), as shown in Fig. 1. The CPT missions were also independently confirmed by the video systems, as shown in Figures 7-8.

V. DISCUSSIONS AND CONCLUSIONS

The SIZ_M algorithm worked well even when the experimental plumes appeared to behavior much differently the modeled plumes on which the algorithms were based. Fig. 6(a)-(b) display the distributions of the LCDPs detected during a simulation test run and the MSN007r2 mission at SCI in November 2000 with the following features. First, most of the LCDPs are clustered in the vicinity of the source locations. Second, the number of the LCPDs is much less than that of the odor-hit points. For example, 4066 odor hit points were detected during the simulation test run, of which only 38 are LCDPs, and 1464 odor-hit points were detected during the NSM007r2 mission, of which only 16 are LCDPs. These characteristics indicate that the source identification algorithm based on the LCDPs is reasonable.

The in-water test runs provide valuable natural flow data for further understanding of some difficulties with tracing the chemical plumes in near-shore ocean environments. First, fluid flow may significantly change its direction in some period, for example, fluid flow had its direction change for about 180° in the period from MSN009 to MSN010r1 of the SCI tests in 2002. The significant change of flow direction might cause a considerable differentiation between the plume axis and the mean flow direction over the period of the REMUS maneuvering. Apparently, the time scale of forming the plume status was significantly different from that of a CPT mission via the REMUS. This indicates that CPT strategies based on the mean flow direction might be not suited to natural fluid environments. Next, the water column in the near-shore ocean may consist of flowing layers in different directions, e.g., the REMUS detected that the top

layer flow was in the opposite direction of the bottom layer flow in the in-water tests of Duck June 2003. Therefore, it was important to control the REMUS to trace the chemical toward its source in the bottom boundary layer. However, lowering the vehicle altitude to trace the plumes had to consider the REMUS-generated altitude errors over ±1.5 m. A low altitude setting controls the REMUS maneuvering in the vicinity of the plume source, but may cause the REMUS to hit the ground.

The simulation studies show that the simulated plume exhibits a significant meander only when it is transported over 30 meters from its source under significant flow variation. It is very important to evaluate CPT strategies using a plume with significant meander. Tracking of a plume within an OpArea with scales of few meters using a laboratory robot could be successful by different "zigzag path" based tracing strategies, and even by a strategy implemented by the simple rules: *if a chemical is detected, the robot moves up-flow*; *if a chemical is lost, the robot moves cross-flow*. However, such an implementation might not work for natural environments.

We abstract the source identification algorithms from the moth-inspired plume-tracing strategies. The optimized moth-inspired strategies reach the success rate of over 95% in tracing plumes. This rate is much higher than that in tracing a pheromone plume of 70% seen in insects in [18]. We introduce a waiting time, λ, into the plume tracing strategies, as chemical plumes developed in a turbulence-dominated fluid environment are highly intermittent. If λ is too small or equal to zero, all odor-hit points could become LCDPs. Consequently, inter-hit distances, which could occur in any part of the plume, cause spurious source identifications. The work [7] studied the effect of λ on plume-tracing performance. Increasing λ gives the vehicle additional time to encounter odor, but can result in the vehicle being significantly further from the plume when it decides that the plume has been lost. Also, note that the improvement of plume tracing saturates as λ increases over 10 s. Considering the REMUS mechanical restrains, we choose λ as 5.0 s – 8.5 s for the moth-inspired CPT strategies.

Fig. 7. A LCPD was detected on the plume tail while the AUV overshooting the source

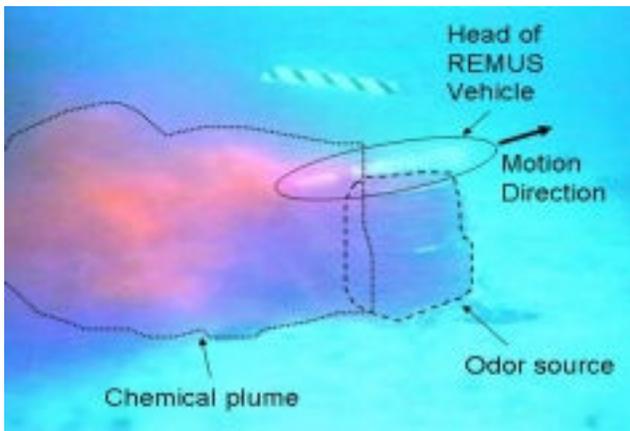
Fig. 8. A LCPD was detected on the plume side while the AUV crossing the plume

Here, we compare the source identification performance achieved by the simulation evaluations and reported by the in-water tests in the three aspects: reliability, accuracy, and identification time cost. The algorithm achieves the high success rates in identifying source locations for both the simulation evaluations and the in-water test runs. The source identification accuracy achieved by the simulation evaluations is higher than the accuracy achieved by the in-water test runs. One reason is that the LCPDs detected during the in-water test runs distributed much more dispersedly than the LCDPs detected during the simulation test runs due to the wide Rhodemine dye plume. The movie clip made by the test director provides an additional evidence of the LCDPs dispersion. Two snapshots captured from the movie clip visually demonstrate two typical LCDPs in the vicinity of the odor source. Figures 7-8 show that the AUV detected a LCDP on a side of the Rhodamine plume when crossing the plume and a LCDP at the tail of the Rhodamine plume when overshooting the odor source, respectively. The analysis in [11] indicated that the SIZ_M algorithm spent much time to identify the sources of the Rhodamine dye plume. In contrast, the corresponding time was much shorter in simulation runs. Our further research will address this problem and propose an approach to filling this gap.

REFERENCES

[1] J. H. Belanger and M. A. Willis, "Adaptive control of chemical -guided location: Behavioral flexibility as an antidote to environmental unpredictability," *Adaptive Behavior*, vol. 4, pp. 217-253, 1998.
[2] F. W. Grasso, T. R. Consi, D. C. Mountain, and J. Atema, "Biomimetic robot lobster performs chemo-orientation in turbulence using a pair of spatially separated sensors: Progress and challenges," *Robotics and Autonomous Systems*, vol.30, pp. 115-131, 2000.
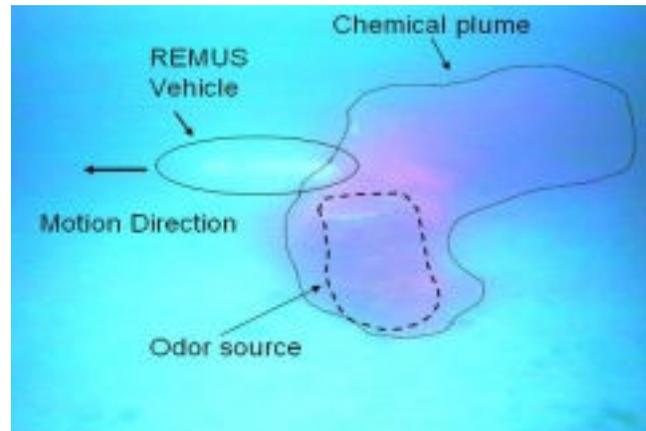[3] F. W. Grasso and J. Atema, "Integration of flow and chemical sensing for guidance of autonomous marine robots in turbulent flows," *Journal of Environmental Fluid Mechanics*, vol. 1, pp. 1-20, 2002.
[4] Q. Liao and E. A. Cowen, "The information content of a scalar plume – A plume tracing perspective," *Environmental Fluid Mechanics*, vol. 2, no. 1-2, pp. 9-34, 2002.
[5] M. J. Weissburg *et al*., "A multidisciplinary study of spatial and temporal scales containing information in turbulent chemical plume tracking," *Environmental Fluid Mechanics*, vol. 2, no. 1-2, pp. 65-94, 2002.
[6] A. T. Hayes, A. Martinoli, and R. M. Goodman, "Distributed chemical source localization," *IEEE Sensors Journal*, vol. 2, pp. 260-271, 2002.
[7] W. Li, J. A. Farrell, and R. T. Cardé, "Tracking of fluid-advected chemical plumes: Strategies inspired by insect orientation to pheromone," *Adaptive Behavior*, vol. 9, pp. 143-170, 2001.
[8] R. A. Russell, D. Thiel, R. Deveza, and A. Mackay-Sim, "A robotic system to locate hazardous chemical leaks," *in Proc. of 1995 IEEE Inter. Conf. on Robotics and Automation*, vol.1, pp.556–561, 1995.
[9] R. A. Russell, "Tracking chemical plumes in constrained environments," *Robotica,* vol. 19, 451–458. 2001.
[10] H. Ishida, Y. Kagawa, T. Nakamoto, and T. Moriizumi, "Chemical-source localization in the clean room by an autonomous mobile sensing system," *Sensors and Actuators B*, vol. 33, pp. 115-121, 1996.
[11] J. Murlis, "The structure of odour plumes," In T. L. Payne, M. C. Birch, and C. E. J. Kennedy (eds.), Mechanisms in insect olfaction, pp.27-38, 1986.
[12] W. Li, J. A. Farrell, S. Pang, and R. M Arrieta, "Moth-inspired chemical plume tracing on an autonomous underwater vehicle", *IEEE Transactions on Robotics*, vol.22, no.2, pp.292-307, 2006.
[13] J. A. Farrell, S. Pang, and W. Li, "Chemical plume tracing via an autonomous underwater vehicle," *IEEE Journal of Ocean Engineering*, vol.30, pp.428-442, 2005.
[14] W. Li, "Abstraction of odor source declaration algorithm from moth-inspired plume tracing strategies", *in Proc. of IEEE Conf. on Robotics and Biomimetics*, pp.1024-1028, 2006.
[15] J. A. Farrell, J. Murlis, X. Long, W. Li, and R. T. Cardé, "Filament-based atmospheric dispersion model to achieve short time-scale structure of chemical plumes", *Environmental Fluid Mechanic*s, vol. 2, pp. 143-169, 2002.
[16] R. T. Cardé, "Odour plumes and odour-mediated flight in insects in olfaction in mosquito-host interactions," in *Proc. CIBA Found. Symp*, pp. 54-70, 1996.
[17] J. S. Elkinton and R. T. Cardé, "Appetitive flight behavior of male gypsy moths (Lepidoptera: Lymantriidae)," *Environmental Entomology,* vol.12, 1702–1707, 1983.
[18] J. H. Belanger and E. A. Arbas, "Behavioral strategies underlying pheromone-modulated flight in moths: lessons from simulation studies," *J. Comp. Physia*, vol. 183, pp. 345-260, 1998.